A new ion–ion plasma thruster with an annular geometry

Stéphane Mazouffre, Denis Renaud

EPJ manuscript No.
(will be inserted by the editor)

A new ion-ion plasma thruster with an annular geometry

Stéphane Mazouffre[1] and Denis Renaud[1]

CNRS, ICARE, EP team, 1c Avenue de la recherche scientifique, 45100 Orléans, France

Received: date / Revised version: date

Abstract. The concept of ion-ion plasma thruster relies on a magnetic filter to create an electron-free plasma in the ion current extraction region. However, experiments and computer simulations show a transverse magnetic field makes the discharge asymmetrical due to electron drift and instabilities in the region of strong magnetic field. The drift drives a large electron flux to the walls, therefore increasing losses, and reduces the electron confinement by creating an escape path throughout the magnetic filter, which is detrimental for the thruster performances. We present a new architecture for an ion-ion plasma thruster that allows to cancel the asymmetry of the plasma by closing in the electron drift on itself. The concept is termed AIPE, an acronym for Annular Ion-ion Plasma Engine. A prototype was developed and tested with noble gases and SF_6. Outcomes of experiments dedicated to the examination of the AIPE discharge and beam by means of Langmuir probe, E×B probe and laser photodetachment are given and discussed. It is shown that the discharge is symmetrical and homogeneous. In addition, positive and negative ions can be extracted and accelerated through the grid assembly.

PACS. 52.75.Di Ion and plasma propulsion – 52.50.Qt Plasma heating by radio-frequency fields; ICR, ICP, helicons – 52.70.m Plasma diagnostic techniques and instrumentation

1 Introduction

Electric propulsion (EP) is at present a well-established technology for moving satellites and spacecraft in space [1–4]. EP allows to achieve a high propellant exhaust speed as a large amount of energy can be transferred to the propellant, which directly translates into a low propellant consumption. Propellant mass economy is the main advantage of EP with respect to chemical propulsion for which acceleration originates in the conversion of chemical energy into kinetic energy through an expansion process. Although electric or ion thrusters deliver a low thrust level due to the current limit in power on-board spacecraft, they are the best options for various types of space maneuvers and missions, such as orbit transfer, trajectory and attitude control, end-of-life deorbit and interplanetary trips, to only name a few [1,3]. There are nowadays a large variety of EP devices and concepts that cover a broad range of sizes, powers, thrusts and ejection speeds. The most advanced and most widely used technologies are the Hall thruster and the gridded ion engine. While Hall thrusters offer a large thrust-to-power ratio, ion engines deliver a great exhaust velocity with a high efficiency and a low beam divergence but the thrust level is limited. The latter are then best suited for missions where the propellant mass and consumption are critical factors such as unmanned deep-space exploration, journeys towards distant celestial bodies and asteroids and propulsion of micro-spacecraft.

The gridded ion engine is an ion accelerator in which the thrust density is achieved through electrostatic interactions [5–9]. The propellant ionization and ion acceleration processes are physically separated in this device, which permits a fine tuning of thrust and exhaust velocity. The thruster geometry is mostly cylindrical. Ionization can be achieved by direct electron impact or by means of high-frequency waves [10]. Ions are extracted and accelerated to high velocity by means of a multi-aperture grid assembly that is commonly composed of two grids. The thrust depends upon the current flowing through the grids and the exhaust velocity is directly given by the potential difference between the grids. Electrostatic neutralization of the extracted ion beam is realized downstream of the grid assembly where electrons from an external cathode, called the neutralizer, mix with the ions to form a quasineutral current-free beam [4–6]. The neutralizer is a critical component of an ion engine. Its malfunctioning leads to a partial ion current neutralization and the resulting space-charge drastically decreases the thruster performances, which, in most cases, means the abort of the mission.

One singular way to eliminate risks linked to the neutralizer is to produce the thrust from an ion-ion plasma instead of an electropositve plasma. As a matter of fact, a gridded ion engine that operates with a strongly electronegative gas as propellant and that ejects pair of positive and negative ions does not require an external neutralizer. The concept of ion-ion plasma thruster has been in-

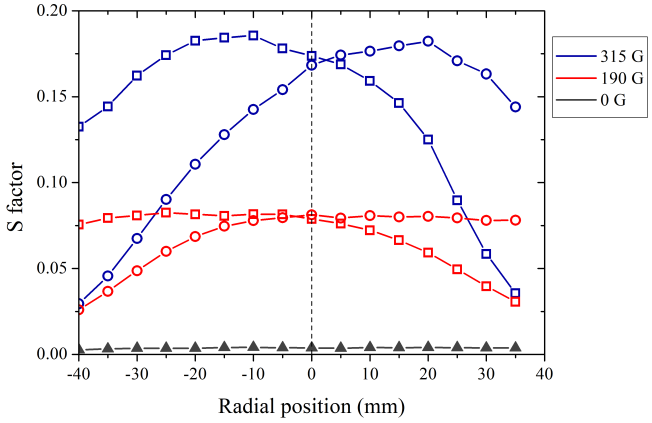

Fig. 1. Distribution of the S factor in the y direction for 3 values of the magnetic field strength. Squares indicate SN configuration of the filter and circles indicate NS configuration. Conditions: 5 sccm SF_6 + 5 sccm Kr, 150 W.

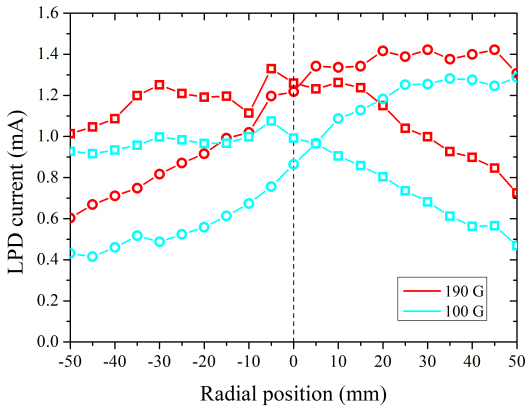

Fig. 2. LPD current as a function of the radial position for 2 values of the magnetic field strength. Squares indicate SN configuration of the filter and circles indicate NS configuration. Conditions: 5 sccm SF_6 + 5 sccm Kr, 150 W.

vestigated in previous years through development, testing and optimization of the PEGASES ion source. PEGASES, an acronym for Propulsion with Electronegative GASES, is an unconventional rectangular Radio-Frequency gridded ion source working with electronegative gases like SF_6 and I_2 [11–14]. Positive and negative ions are alternately accelerated using a square-wave voltage waveform. The validity of the concept, especially the production of a high-density ion-ion plasma and the alternate ejection of positive and negative ions with large velocities, has been demonstrated [15–18]. However, visual inspection, camera imaging and recent works performed by means of Langmuir probes and laser photodetachment have revealed a distinct asymmetry in the plasma distribution inside the thruster cavity when a magnetic filter is installed [19]. As we shall see, the asymmetry originates from the existence of an open electron drift in the magnetic barrier, which results in an escape path for the electrons, hence destroying the confinement and creating inhomogeneous losses. In this contribution we describe a novel design for an ion-ion plasma thruster that eliminates the asymmetry, therefore potentially increasing the performances. The main difference with the original concept is that the source geometry is annular with inner and outer magnetic poles whereas it is rectangular for PEGASES with external magnets only.

2 Asymmetry with a rectangular geometry

Inhomogeneous light distribution as well as asymetry in plasma properties and charged particle currents have been observed and studied in several low-pressure partly magnetized discharges operating with electropositive as well as electronegative gases [20–23]. The key factor for generating an asymmetry is the magnetic field topology. The asymmetry is present when a magnetic barrier, or magnetic filter, is used. Magnetic field lines are in that case perpendicular to the current and gas flow direction and they intercept the walls. PEGASES is an example of plasma source that rests upon a magnetic filter. An inductively-coupled RF discharge is produced in a 12 cm in length, 10 cm in width and 6 cm in heigth cavity with dielectric walls [13,14,17]. The injected electronegative gas is efficiently ionized at the back of the cavity by means of a planar antenna embedded into a ferrite shield that is operated around 4 MHz. The input RF power ranges between 80 W and 250 W. In the ionization region, the plasma is composed of electrons as well as positive and negative ions. Permanent magnets are used to generate the transverse **B** of the filter of which the magnitude can be ramped up to 340 G by varying the number of magnets. The filter traps electrons and therefore enhances the production of negative ions by cooling down the electron fluid through collisions with neutrals. Downstream the filter the plasma mostly contains positive and negative ions. The ion-ion plasma is extracted and accelerated using two planar metal grids with a transparency of 60%. The first grid is polarized to a high potential to elevate the plasma potential in the dielectric cavity and the second grid is grounded. Positive and negative ions are alternately accelerated using a square-wave voltage waveform of which the frequency is close to the ion-ion plasma frequency.

The inhomogeneous plasma distribution in the PEGASES thruster cavity has first been observed by the naked eyes without the grid assembly. Afterwards camera imaging has allowed a more accurate investigation of the light distribution [19,24]. More recently the asymmetry has been examined using Langmuir probes as well as the laser photodetachment technique. Figure 1 illustrates outcomes of measurements carried out with a 0.2 mm in diameter and 3 mm long platinum cylindrical probe. Instead of extracting the negative ion properties from the probe current-voltage characteristic curve, we computed the so-called symmetry factor. The S factor is defined as the ratio of saturation current of positive ions to saturation current of negative charges, i.e. electrons and negative

ions:

$$S = \frac{I^+}{I^- + I_e}. \quad (1)$$

This ratio images the symmetry of the probe I-V curve. In the case of an ideal ion-ion plasma, i.e. when positive and negative ions have the same mass and the same temperature, the ratio is 1. The ratio tends to 0 for an electropositive plasma. Plots in Fig. 1 were obtained with an open cavity at the grid location ($x = 12$ cm, where 0 refers to the back of the cavity) with a gas mixture of 5 sccm SF_6 and 5 sccm Kr and 150 W of RF input power. The filter was placed at $x = 7$ cm, i.e. in the middle of the cavity. The magnetic field direction could be changed from NS to SN by inverting the magnets [24]. Without magnetic filter, the S factor stays constant at 0.004 across the cavity. The effect of the filter in terms of negative ion production is obvious in Fig. 1. The S factor increases with B that means the fraction of negative ions increases, in agreement with other data [17,19]. The S factor profile is, however, not symmetrical in the y-direction with respect to the cavity axis. Besides, the S factor curve reverses with the **B**-field direction.

Other series of experiments have been performed using Laser PhotoDetachment (LPD). LPD is a non-intrusive technique that allows to detect negative ions A^- and to determine the local plasma electronegativity α [25–27]. The principle behind the LPD technique is relatively straightforward. When a negative ion is illuminated with a laser beam, the electron is detached if the photon energy is above the binding energy, the so-called electron affinity. The LPD can be summarized through the following equation:

$$A^- + h\nu \longrightarrow A + e^-, \quad (2)$$

where A is a neutral atom and e an electron. LPD therefore transforms the negative ion density into an electron density. The latter can be measured by means of a Langmuir probe, a Hairpin probe or microwave interferometry. For weakly electronegative plasmas, the sudden change in the electron current due to the laser pulse does not disturb the local equilibrium, therefore the electronegativity and the negative ion absolute number density n^- can be assessed from the LPD signal. However, when the plasma is highly electronegative, or ion-ion, the change in plasma and sheath dynamics driven by the laser pulse prevents from easily extracting α and n^- from the LPD signal and one must turn towards complicated numerical simulations [28–30]. In this work we therefore solely consider the LPD signal, i.e. the electron current variation after laser illumination. Our LPD setup is extensively described in [17,31]. Only a brief description is given here. The optical bench is based on a 10 Hz 8 ns pulse duration Nd-YAG laser at 1064 nm. Second harmonic generation crystals produce 4.65 eV photons with a wavelength of 266 nm that can detach electrons from all negative fragments in a SF_6 plasma. The energy can be varied between 0 and 28 mJ per pulse by changing the laser beam polarization. A 150 cm focal length UV lens creates a 2 mm spot size at the measurement location. The laser fluence stays below 0.5 J/cm^2 to avoid material ablation. A L-shape Pt Langmuir probe

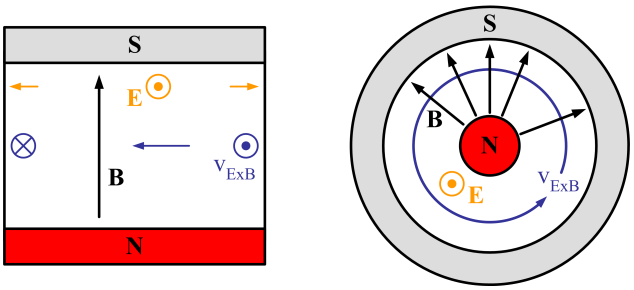

Fig. 3. **E**×**B** drift in rectangular and annular geometries.

with dimensions similar to the one used for the S factor studies collects photodetached electrons. A L-shape probe was selected to minimize laser-induced sputtering, to be perpendicular to the magnetic field lines and to warrant a full coverage by the light beam. The probe is mounted onto a translation stage for measurements in the x and y direction. The probe is positively biased well above the local plasma potential. LPD experiments show F^- is the dominant negative ion in agreement with E×B probe measurements [17]. They also reveal the negative ion content is maximum for a 50/50 SF_6-Kr mixture just as a SF_6-Ar mixture [18]. The profile of the LDP current along the y-direction of the PEGASES cavity is displayed in Fig. 2 for two magnitudes of the B-field in NS and SN configurations. The experimental conditions were 5 sccm SF_6 plus 5 sccm Kr gas mixture and 150 W RF power. Measurements have been realized 5 cm downstream the cavity exit plane ($x = 17$ cm) without the grids. The LPD current increases with the **B**-field magnitude. An asymmetry that depends on the field direction is visible in Fig. 2. The LPD current and S factor radial distributions are qualitatively in perfect agreement: they both indicate the region where the negative ion density is the largest.

The asymmetry observed in the S factor and LPD current radial profiles as well as in the light and plasma properties distribution is a general phenomenon for conventional low-pressure discharges with a magnetic filter. The asymmetry originates in the existence of an **E**×**B** electron drift due to the interaction between the applied transverse magnetic field and the electric field associated with the plasma potentiel drop in the wall pre-sheath and sheath, as shown in various experimental and numerical works [20–23,32,33] . The **E**×**B** drift weakens the magnetic confinement and it permits electron to escape in the downstream region, hence attenuating the effect of the filter.

3 Annular geometry

The asymmetry can be eliminated by moving from a rectangular or cylindrical cavity geometry, the traditionnal design, to an annular geometry as the transformation modifies the plasma boundary conditions in the y-direction perpendicular to the **B** field lines, as exemplified in Fig. 3. The electron **E**×**B** drift near the walls vanishes with an annular geometry. Although a drift is present due to the

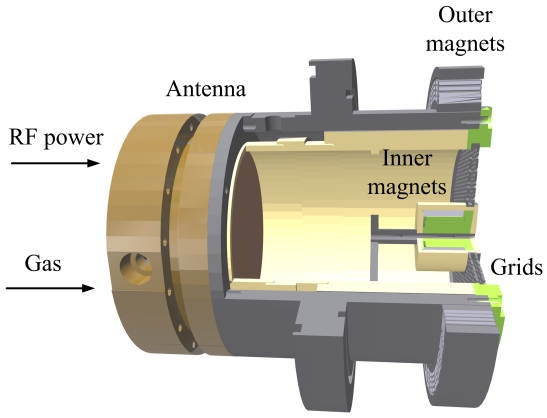

Fig. 4. CAD of the AIPE thruster prototype.

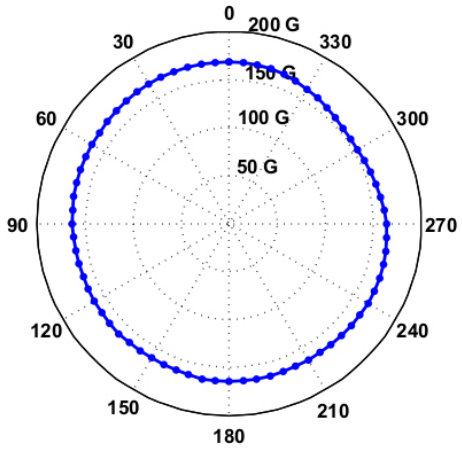

Fig. 5. Polar graph of the magnetic field strength at $x = 10\,\text{cm}$ on the mean cavity radius.

axial potential gradient, it returns on itself. The annular architecture therefore allows to move from an open to a close $\mathbf{E}\times\mathbf{B}$ drift, which makes plasma properties homogeneous in the azimuthal direction.

The architecture of the annular geometry ion-ion plasma thruster, which has recently been patented [34], is depicted in Fig. 4. Contrary to classical negative ion sources, this source, called AIPE for "Annular Ion-ion Plasma Engine", has a design based upon a solid of revolution with inner and outer magnetic poles to produce a magnetic barrier similar to the one of Hall thrusters [1,4]. The cavity of the AIPE prototype is cylindrical in the electronegative plasma region where the power is deposited whereas it is annular in the magnetized region where the ion-ion plasma is formed. The cavity side walls are made of BN-SiO_2. The external wall is 94 mm in inner diameter and 120 mm in length. The internal wall is 36 mm in outer diameter and 30 mm long. The mean radius in the annular section is then 32.5 mm. Sizes have been selected to obtain a short mean free path for the electron attachment reaction within the ionization region. The back of the cavity is a thin alumina disk that protects the RF antenna from the plasma. The gas is injected through eight 1 mm in diameter apertures bored in the external ceramic wall. The holes are located at $x = 2\,\text{cm}$. The $x = 0\,\text{mm}$ position refers to the back of the cavity. They are azimuthally distributed and equally spaced. A highly porous mullite ceramic protects the holes by screening the plasma and avoids short-circuits with the metal injection line. Currently the AIPE concept relies on an inductively coupled RF plasma discharge. The RF power is transferred to the propellant gas thanks to a 7-loop circular copper coil embedded in a zinc-nickel ferrite. The magnetic field is created by 150 small rectangle SmCo magnets divided between the internal and the external pole. The maximum strength of the magnetic field is 170 G. The highest B field is reached at $x = 10\,\text{cm}$. Figure 5 is a polar plot of the magnetic field magnitude at $x = 10\,\text{cm}$ on the mean radius of the annular section. The magnetic field intensity is constant but around 300° where it reaches ∼150 G. The defect may originate in a misalignment of the magnets at this location. Besides, the dimensions of the magnets are not strictly indentical, which leads to a 4% uncertainty level. This is comparable to the measured variation. Notice the magnets are extremely fragile and they can easily be deteriorated during manipulation, which represents another possible source of $\mathbf{B}$ field magnitude variation. The acceleration stage is composed of two stainless-steel grids. The gap between them is 2 mm. The hole diameter is 2 mm. The transparency is 58 %. The first grid is located at $x = 12$ cm, i.e at the exit plane of the cavity. Contrary to PEGASES, the extraction grid is close to the maximum of the magnetic field strength, where the negative ion density is the highest as demonstrated by laser photodetachment measurements [19]. The screen (first) grid is polarized at a high voltage with alternate polarity in order to extract positive and negative ions in turns. The power supply can deliver an output voltage up to ± 1000 V with a frequency ranging from 0 up to 37 kHz. The acceleration (second) grid is grounded.

In this work, the AIPE thruster has been operated at 4.0 MHz with a tunable circuit for impedance matching. The power transfer efficiency reached 0.65 for a RF input power between 100 W and 180 W and with a total gas flow rate of 10 sccm. The gas pressure inside the cavity was $\sim 10^{-3}$ mbar under these conditions. A front view picture of the AIPE prototype without grids firing with krypton is shown in Fig. 6. The thruster has been tested in a 0.5 m in diameter and 0.8 m in length cylindrical vacuum tank evacuated by a 1000 l/s turbomolecular pump connected to a 65 m^3/h primary pump. The background pressure inside the chamber is typically 2×10^{-4} mbar during operation. The AIPE thruster is mounted at one end of the chamber by means of a KF200 flange. The three holders of the internal pole are clearly visible in Fig. 6. The plasma is homogeneous and symmetrical, despite variations in the magnetic field magnitude. As can be seen, the largest plasma density, which corresponds to the largest light intensity, is reached in the vicinity of the internal pole.

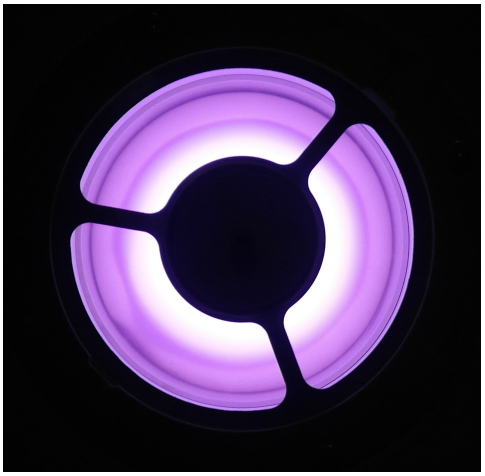

Fig. 6. Photograph of AIPE thruster operating with 10 sccm of Kr at 140 W. Grids have been removed.

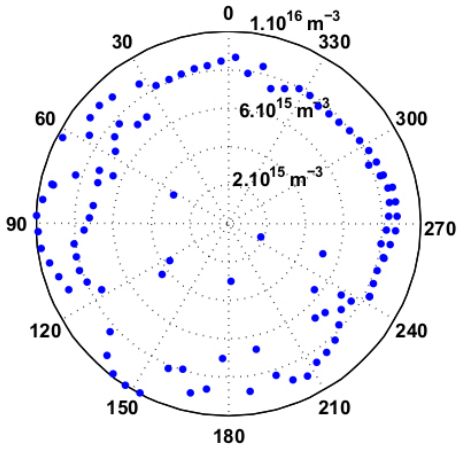

Fig. 7. Polar plot of the electron density in m^{-3} at $x = 13$ cm on the annular cavity mean radius (10 sccm Kr, 100 W).

4 Plasma discharge characteristics

4.1 Electropositive plasma

The AIPE prototype has first been operated with krypton to verify proper functionning of the ICP source and to easily determine the electron properties. Langmuir probe measurements have been performed 1 cm downstream the cavity exit plane, i.e. at $x = 13$ cm, without installing the grids. The electron properties were therefore examined in the extraction region of the thruster. The probe tip is a 0.2 mm in diameter and 5 mm long tungsten wire. The probe holder is a 2 mm in diameter alumina tube. The probe is mounted onto a rotation stage in order to carry out measurement in the azimuthal direction with the tip perpendicular to the magnetic field lines. The probe current-voltage characteristic curves have not been corrected for the presence of a magnetic field. The **B** field strength is ≈16 G in the measurement area that means the electron Larmor radius is around 2 mm, much larger than the probe radius. The plasma potential V_p corresponds to the maximum of the first derivative of the I-V curve. The electron density n_e was determined using the OML theory, that means deduced from the slope of the $I_e^2 = f(V)$ plot. The electron energy distribution function is here assumed to be Maxwellian. The electron temperature T_e is then inferred from the slope of the $Ln(I_e)$ plot between V_f and V_p after substracting the ion current.

Figure 7 shows the electron density at $x = 13$ cm on the annular cavity mean radius as a function of the angle. The thruster was operated with 10 sccm of krypton and 100 W of RF input power. The electron density is relatively homogeneous in the azimuthal direction with a mean value of $7{\times}10^{15}$ m^{-3}. The number density in the extraction region is very low compare to density in the ionization region where n_e reaches about $5{\times}10^{17}$ m^{-3}. Figure 8 gives the azimuthal distribution of the electron temperature at $x = 13$ cm on the mean radius. The graph reveals the temperature is homogeneous with a mean value around 0.5 eV. For comparison, the electron temperature in the ionization region close to the antenna is around 5 eV. The azimuthal distribution of the two quantities n_e and T_e is in agreement with visual observation of the discharge, see Figure 6. With an electropositive plasma, an annular ion-ion plasma thruster produces an homegeneous and isotropic plasma in the drift direction.

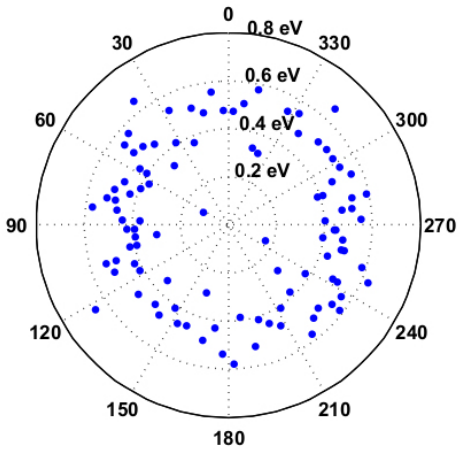

Fig. 8. Polar plot of the electron temperature in eV at $x = 13$ cm on the annular cavity mean radius (10 sccm Kr, 100 W).

The electron density and temperature profiles in the axial direction are displayed in Fig. 9 for several azimuthal angles. Measurements have been carried out in the annular region without the grid assembly. The noticeable increase in density around $x = 10$ cm is likely a direct consequence of the gas pressure increase due to the narrowing of the cross-section. The large drop in electron density and electron temperature behind $x = 10$ cm demonstrates the efficiency of the magnetic filter, a key aspect for producing a high-density ion-ion plasma from an electronegative gas.

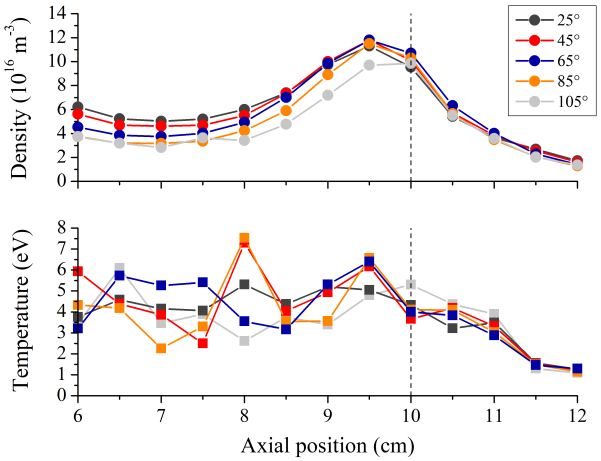

Fig. 9. Electron density and temperature against x in the annular region for several angles (10 sccm Kr, 100 W). The dashed line indicates the location of the magnetic filter.

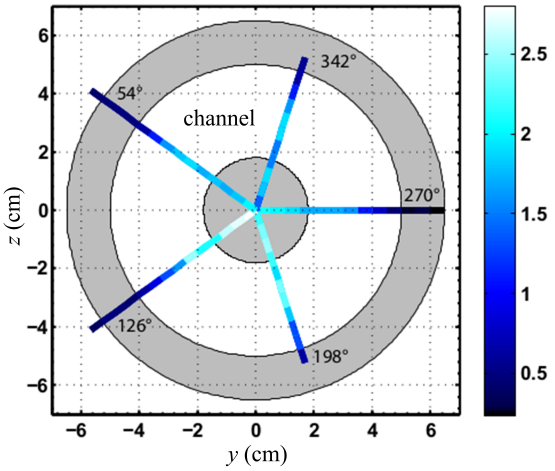

Fig. 10. LPD current in mA measured along the thruster radius 1 cm behind the exit plane ($x = 13$ cm) for various angles (without grids, 5 sccm SF_6 + 5 sccm Kr, 140 W RF power).

4.2 Electronegative plasma

In a second phase, the AIPE prototype has been operated with SF_6 to investigate the negative ion production behind the magnetic filter.

Figure 10 shows the laser photodetachment current, i.e. the relative amount of negative ions, along the thruster radius at several angular positions. LPD measurements have been carried out 1 cm downstream the exit plane ($x = 13$ cm) without the grid assembly. The 266 nm laser beam propagated in the horizontal plane that contains the thruster axis and it was parallel to the cavity exit plane. The L-shape Pt Langmuir probe was mounted onto a translation stage to enable measurements in the y-direction. The azimuthal angle was varied by rotating the entire thruster assembly. The thruster was operated with a gas flow rate composed of 5 sccm SF_6 plus 5 sccm Kr. The RF input power was set at 140 W. The largest LPD current is captured in the AIPE thruster channel, as can be seen in Fig. 10. The LPD signal is high even in the region of strong light emission, see the picture in Fig. 6. The LPD current diminishes a bit when moving towards the edge of the external thruster wall, whatever the angle. Figure 10 indicates the plasma is symmetrical and homogeneous when AIPE operates with an electronegative gas.

Langmuir probe current-voltage traces have also been used to compute the symmetry factor S. Figure 11 presents the evolution of the symmetry factor in the radial direction for different angles at $x = 13$ cm. Experimental conditions were similar to the ones used for LPD measurements. The plasma discharge is seemingly weakly electronegative in the central region where the LPD signal is the strongest. It is stongly electronegative near the edge of the thruster cavity. Contrary to what one might think, there is no contracdiction between the S factor and the LPD current maps. The S factor distribution agrees with the light intensity distribution displayed in Fig. 6. As the electron density and temperature are certainly high in the vicinity of the internal pole, the electron current is much larger

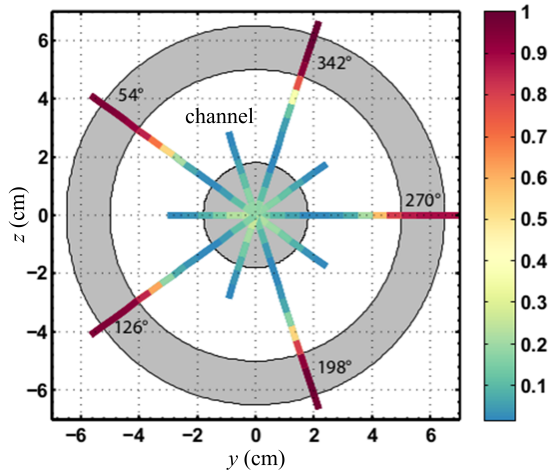

Fig. 11. Symmetry factor SF along the thruster radius 1 cm behind the exit plane ($x = 13$ cm) for many angles (without grids, 5 sccm SF_6 + 5 sccm Kr, 140 W RF power).

than the ion currents, hence a low S factor close to 0.1 in this zone. The opposite holds for the external pole region. Figures 11 and 10 are other evidences that the plasma discharge is homogeneous with a closed electron drift design and that negative ions can be produced in an annular geometry source.

5 Ion extraction and acceleration

After mounting the extraction and acceleration grids, a calibrated E×B probe has been employed to detect the various ions, to determine their relative fraction and to measure their ejection velocity. An E×B probe, also called a Wien filter, is a diagnostic tool that allows to discriminate charged particles with distinct velocity in a particular direction. The basic principle of the probe rests on the

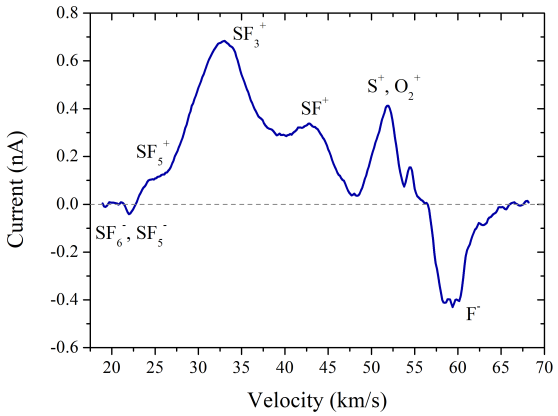

Fig. 12. E×B spectrum acquired in the ion beam of the AIPE thruster at y = 30 mm and +90° (6 sccm SF_6, 140 W and ± 400 V at 1 kHz).

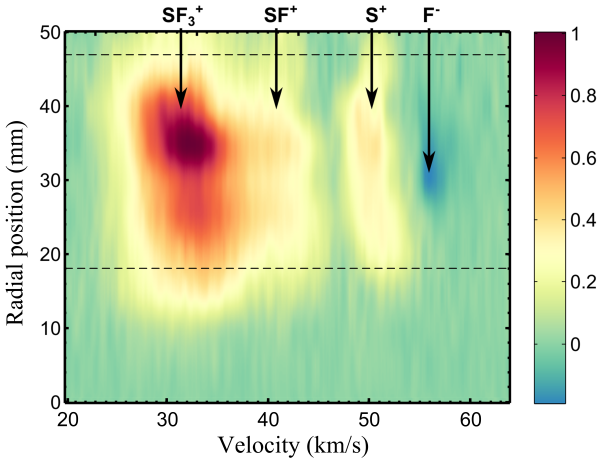

Fig. 13. E×B spectrum series as a function of the radial position y acquired at x = 34 cm and +90° (6 sccm SF_6, 140 W and ± 400 V at 1 kHz). Dashed lines indicate the channel boundaries.

drift of ions in a region of crossed electric and magnetic fields. The magnetic field is fixed inside the device by using permanent magnets. Two electrodes allows to change the electric field by varying the applied potential. When particles undergo no force in the cross-field region, i.e. the Lorentz force is zero, the particle velocity v is given by:

$$v = \frac{E}{B} = \frac{V}{dB}, \tag{3}$$

where E and B are the electric and magnetic field amplitude respectively, d is the distance between electrodes and V the applied voltage on the probe. Sweeping the electrode voltage and collecting the charged-particle current allows to construct the ion velocity distribution function. Further information about an E×B probe principle, architecture and operation can be found in [17] and references herein.

The E×B probe was installed on a translation stage in the horizontal plane that includes the thruster axis to get spatial resolution in the y-direction. The entrance of the probe collimator was placed 22 cm behind the thruster exit plane. Figure 12 shows a calibrated probe spectrum acquired at r = 30 mm and θ = 90°. The AIPE operating conditions were 6 sccm of SF_6, 140 W of RF power and ± 400 V acceleration voltage at 1 kHz. The E×B spectrum was corrected using a calibration parameter as described in [17,31]. The spectrum is similar to the one obtained with the PEGASES thruster under identical conditions, in particular positive and negative ions are the same. The main difference is the quantity of SF_3^+ and F^- ions that is larger in the case of the AIPE prototype. Consequently, the average ion mass is 76 a.m.u. for AIPE and 51 a.m.u. for PEGASES thruster. A larger average mass is beneficial for space propulsion.

A series of E×B spectra as a function of the radial position recorded at x = 34 cm and +90° is shown in Fig. 13 for a pure SF_6 plasma discharge in the form of a contour plot. Operating conditions were similar to the ones of Fig. 12. The experimental spectra show the AIPE thruster

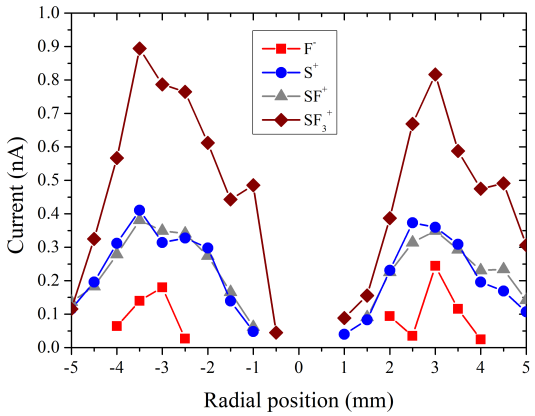

Fig. 14. Current as a function of the radial position for various ions measured with the E×B probe at +90° and -90° (x = 34 cm, 6 sccm SF_6, 140 W and ± 400 V at 1 kHz).

can extract positive and negative ions and accelerate them to high velocity without an external neutralizer. Spectra are nearly identical inside the cavity channel, i.e. between y =18 mm and y =47 mm. Negative ions are solely captured around the channel centerline (r =32.5 mm). The largest ion current, that corresponds to the SF_3^+ ion peak, is also measured nearby the channel axis. Figure 13 shows a very low amount of flowing ions beyond the edge of the channel. This fact demonstrates the ion beam divergence angle is small, which is always the case for gridded ion sources. Data in Fig. 13 gives a ∼ 6 ° angle. The peak current measured with the E×B probe is plotted as a function of the radial position in Figure 14 for several ions. Measurements have been performed on both sides of the inner pole, namely at +90° and -90°. The two current profiles are symmetrical, a direct proof for the azimuthal homogeneity of the plasma in the ion beam.

6 Conclusion

A new architecture for a gridded ion-ion plasma thruster has been proposed, built and tested. The cavity geometry is annular with a radial magnetic field in order to close on itself the electron E×B drift. The prototype, which is termed AIPE for "Annular Ion-ion Plasma Engine", is a RF inductively-coupled plasma source using electronegative gases as propellant. As expected, the annular architecture allows to obtain a homogeneous and isotropic plasma in the drift direction contrary to the original rectangular PEGASES thruster design. The discharge properties have been examined at the exit plane with a Langmuir probe and the Laser Photo-Detachment technique. Probe and LPD measurements reveal the azimuthal symmetry of the discharge. The ion beam has been diagnosed with a compact calibrated E×B probe. Positive and negative ions are efficiently extracted and accelerated. The tool also show the azimuthal symmetry of the ion beam for all fragments and it indicates the divergence angle is low.

7 Acknowledgments

Denis Renaud benefits from a Ph.D. grant from AIRBUS DS - R&T - Innovative Electrical Propulsion project.

References

1. S. Mazouffre. Electric propulsion for satellites and spacecraft: established technologies and novel approaches. *Plasma Sources Sci. Technol.*, 25:033002, 2016.
2. M. Martínez-Sánchez and J.E. Pollard. Spacecraft electric propulsion – An overview. *J. Propul. Power*, 14:688–699, 1998.
3. W.P. Wright and P. Ferrer. Electric micropropulsion systems. *Progress in Aerospace Sciences*, 74:48–61, 2015.
4. D. M. Goebel and I. Katz. *Fundamentals of Electric Propulsion.* . Wiley, Hoboken, NJ, 2016.
5. D. M. Goebel and I. Katz. *Physics of Electric Propulsion.* . McGraw-Hill, New York, 1968.
6. P.J. Wilbur, V.K. Rawlin, and J.R. Beattie. Ion thruster development trends and status in the United States. *J. Propul. Power*, 14:708–715, 1998.
7. D.M. Goebel, R.E. Wirz, and I. Katz. Analytical ion thruster discharge performance model. *J. Propul. Power*, 23:1055–1067, 2007.
8. K.H. Groh and H.W. Loeb. State of the art of radiofrequency ion sources for space propulsion. *Rev. Sci. Instrum.*, 65:1741–1744, 1994.
9. L.T. Williams and M.L.R. Walker. Ion production cost of a gridded helicon ion thruster. *Plasma Source Sci. Technol.*, 22:055019, 2013.
10. H.W. Loeb. Plasma-based ion beam sources. *Plasma Phys. Control. Fusion*, 47:B565–576, 2005.
11. A. Aanesland, A. Meige, and P. Chabert. Electric propulsion using ion-ion plasmas. *J. Phys.: Conf. Ser.*, 162:012009, 2009.
12. A. Aanesland, S. Mazouffre, and P. Chabert. PEGASES A new promising electric propulsion concept. *Europhys. News*, 42:28–31, 2011.
13. D. Rafalskyi, L. Popelier, and A. Aanesland. Experimental validation of the dual positive and negative ion beam acceleration in the plasma propulsion with electronegative gases thruster. *J. Appl. Phys.*, 115:053301, 2014.
14. A. Aanesland, D. Rafalskyi, T. Lafleur, P. Grondein, P. Chabert, S. Mazouffre, D. Renaud, L. Garrigues, G.J.M. Hagelaar, and D. Levko. Development and test of the negative and positive ion thruster PEGASES. In *Proceedings of the 50th Joint-Propulsion Conference*, AIAA Paper 2014-3424, Cleveland, Ohio, 2014.
15. D. Levko, L. Garrigues, and G.J.M. Hagelaar. Transport of low pressure electronegative SF6 plasma through a localized magnetic filter. *Phys. Plasmas*, 21:083505, 2014.
16. T. Lafleur, D. Rafalskyi, and A. Aanesland. Alternate extraction and acceleration of positive and negative ions from a gridded plasma source. *Plasma Sources Sci. Technol.*, 24:015005, 2015.
17. D. Renaud, D. Gerst, S. Mazouffre, and A. Aanesland. E B probe measurements in molecular and electronegative plasmas. *Rev. Sci. Instrum.*, 86:123507, 2015.
18. A. Aanesland, D. Rafalskyi, J. Bredin, P. Chabert P. Grondein, N. Oudini, D. Levko, L. Garrigues, and G.J.M. Hagelaar. The PEGASES gridded ionion thruster performance and predictions. *IEEE Trans. Plasma Sci.*, 43:321–326, 2015.
19. D. Renaud, E. Pawelec, and S. Mazouffre. Investigation of the PEGASES thruster magnetic filter via laser photodetachment experiments. In *Proceedings of the 34th International Electric Propulsion Conference*, IEPC paper 2015–380, Hyogo-Kobe, Japan, 2015.
20. D. Gerst, S. Cuynet, M. Cirisan, and S. Mazouffre. Plasma drift in a low-pressure magnetized radio frequency discharge. *Plasma Sources Sci. Technol.*, 22:015024, 2013.
21. F. Gaboriau, R. Baude, and G.J.M. Hagelaar. Experimental evidence of the increased transport due to the wall bounded magnetic drift in low temperature plasma. *Appl. Phys. Lett.*, 104:214107, 2014.
22. P. Hazarika, M. Chakraborty, B. K. Das, , and M. Bandyopadhyay. A technique to control cross-field diffusion of plasma across a transverse magnetic field. *Phys. Plasmas*, 23:122105, 2016.
23. M.B. Thomas, D. Rafalskyi, T. Lafleur, and A. Aanesland. Experimental investigation of electron transport across a magnetic field barrier in electropositive and electronegative plasmas. *Plasma Sources Sci. Technol.*, 25:045018, 2016.
24. D. Gerst. *Investigation of magnetized radio-frequency plasma sources for electric space propulsion.* PhD thesis, University of Orléans, France, 2013.
25. F. El Balghiti-Sube, F.G. Baksht, and M. Bacal. Photodetachment diagnostics of plasma with a high n-/ne ratio. *Rev. Sci. Instrum.*, 67:2221–2227, 1996.
26. M. Bacal. Photodetachment diagnostic techniques for measuring negative ion densities and temperatures in plasmas. *Rev. Sci. Instrum.*, 76:3981–4006, 2000.
27. J. Conway, N. Sirse, S.K. Karkari, and M. M. Turner. Using the resonance hairpin probe and pulsed photodetachment technique as a diagnostic for negative ions in oxygen plasma. *Plasma Sources Sci. Technol.*, 19:065002, 2010.
28. N. Oudini, F. Taccogna, A. Bendib, and A. Aanesland. Numerical simulations used for a validity check on the laser induced photo-detachment diagnostic method in electronegative plasmas. *Phys. Plasmas*, 21:063515, 2014.

29. N. Oudini, N. Sirse, R. Benallal, F. Taccogna, A. Aanesland, and A. Bendib. Numerical experiment to estimate the validity of negative ion diagnostic using photodetachment combined with Langmuir probing. *Phys. Plasmas*, 22:073509, 2015.
30. N. Oudini, N. Sirse, F. Taccogna, A.R. Ellingboe, and A. Bendib. Photo-detachment signal analysis to accurately determine electronegativity, electron temperature and charged species density. *Appl. Phys. Lett.*, 109:124101, 2016.
31. D. Renaud. *Caractérisation du propulseur PEGASES : diagnostic du filtre magnétique et du faisceau ; optimisation de la géométrie*. PhD thesis, University of Orléans, France, 2015.
32. G J M Hagelaar and N Oudini. Plasma transport across magnetic field lines in low-temperature plasma sources. *Plasma Phys. Control. Fusion*, 53:124032, 2011.
33. St. Kolev, G.J.M Hagelaar, G. Fubiani, and J-P. Boeuf. Physics of a magnetic barrier in low-temperature bounded plasmas: insight from particle-in-cell simulations. *Plasma Sources Sci. Technol.*, 21:025002, 2012.
34. S. Mazouffre and D. Renaud, july 7, 2017. Patent FR 3046520.